Predicting Sit-to-Stand Adaptations Due to Muscle Strength Deficits and Assistance Trajectories to Complement Them Using Simulations

KYUTECH-LSSE-18899033

Doctoral Dissertation

Predicting Sit-to-Stand Adaptations Due to Muscle Strength Deficits and Assistance Trajectories to Complement Them Using Simulations

Vinay Kumar

Kyutech

Department of Life Science and Systems Engineering
Graduate School of Life Science and Systems Engineering
Kyushu Institute of Technology

June, 2022

A Doctoral Disseration
submitted to Graduate School of Life Science and Systems Engineering,
Kyushu Institute of Technology
in partial fulfillment of the requirements for the degree of
Doctor of Engineering

Vinay Kumar

Thesis Committee:

Professor Tomohiro Shibata	(Supervisor)
Professor Sozo Inoue	(Co-supervisor)
Professor Hiroaki Wagatsuma	(Co-supervisor)
Professor Tomoya Tamei	(External Reviewer)

Declaration

It is certified that the dissertation has been written entirely by me, not plagiarized from any sources, and describes my work. Specifically:

- Work published by others is not claimed as my original.
- Excerpts (including figures, tables etc.) have not been taken from any section of earlier thesis (including introduction & literature review or other similar sections).
- Due credit has been given to prior work (both published and unpublished) being used or described in the thesis.
- Prior approval has been obtained for the copyrighted works included in this thesis.

Vinay Kumar
KYUTECH-LSSE-18899033

Acknowledgement

I am very grateful to my guide Prof. Tomohiro Shibata for enthusiastically guiding me throughout the doctoral program. I am thankful to Prof. Shuhei Ikemoto and Takahide Yoshiike for their time discussing different aspects of my research and Prof. Tomoya Tamei for sharing the experimental data with us. I would also like to express my gratitude for the feedback provided by Prof. Sozo Inoue, Prof. Hiroaki Wagatsuma, and Prof. Tomoya Tamei towards improving this thesis and the communication of the work within.

Predicting sit-to-stand adaptations due to muscle strength deficits and assistance trajectories to complement them using simulations*

Vinay Kumar

Abstract

Sit-to-stand (STS) transition is one of the most bio-mechanically challenging task necessary for performing activities of daily life. With muscle strength being the most dominant, many co-occurring factors influence how individuals perform STS. This work investigated the STS changes and the STS failure caused by muscle strength deficits using the trajectories generated employing open-loop single shooting optimization and musculoskeletal models. It also presents the external assistance trajectories that can complement strength deficits for successful STS transition using the same framework. The muscle strength deficits were introduced by simultaneously scaling the maximum isometric strength of muscles in steps of 20%. The optimization could generate successful STS transition for models with up to 60% strength deficits. The joint angle, muscle activation and ground reaction force trajectories for the 0% strength deficit model's STS transition agree with those experimentally observed for a healthy adult. Comparison of different strength deficit trajectories shows that when the vasti muscle gets saturated, the activation of antagonistic hamstrings muscles reduces to relieve it. The reduction in hamstring muscle activation subsequently increases the load on the gluteus maximus muscle. This adaptation and the motion tracking results are used to suggest the vastus muscle weakness to be responsible for STS breakdown. Finally, the successful STS trajectory generated for the externally assisted 80% strength deficit model is presented. The trajectory features utilization of external assistance as and when needed to complement strength deficits for successful STS transition. Our results will help plan intervention and design novel STS assistance devices.

Keywords: Sit-To-Stand, Musculoskeletal Model, Strength Deficit, Single Shooting Optimization, Open Loop Controller, Assist-As-Needed

*Doctoral Dissertation, Graduate School of Life Science and Systems Engineering, Kyushu Institute of Technology, KYUTECH-LSSE-18899033, Wednesday 1st June, 2022.

Overview

This dissertation is organized into five chapters.

- Chapter 1 introduces the goals of this study in the context of literature and highlights their novelties.
- Chapter 2 details the human musculoskeletal model used in this study.
- Chapter 3 details the optimization framework used to generate sit-to-stand trajectories.
- Chapter 4 details the motion tracking setup used the analyze the sit-to-stand failure and the steps used to process the experimental data.
- Chapter 5 highlights the findings of this study and contrasts them again literature.
- Chapter 6 concludes this dissertation with a summary of findings, identified limitations, and promising future research directions.

Contents

List of Figures **xiii**

List of Tables **xv**

List of Symbols **xvii**

1 Introduction **1**

2 Human Model **5**
2.1 Modelling simplifications 5

3 Optimization Framework **9**
3.1 Optimization Setup 9
3.2 Cost Function 10

4 Analysis Tools **17**
4.1 Experimental Data Processing 17
4.2 Motion Tracking Setup 18

5 Results **23**
5.1 Unassisted STS Trajectory of 0% Strength Deficit Model 23
5.2 STS Adaptations and Failure 25
5.3 Externally Assisted STS Transition 25

6 Conclusion **33**

Bibliography **35**

Publication List **39**

List of Figures

2.1 **(A)** A planar musculoskeletal model for sit-to-stand. The model's musculotendon actuators (red lines) represents the major uniarticular and biarticular muscle groups that drive the sit-to-stand motion in the sagittal plane, i.e., iliopsoas (ILPSO), gluteus maximus (GMAX), biarticular rectus femoris (RF), biarticular hamstrings (HAMS), vasti (VAS), gastrocnemius (GAS), soleus (SOL), and tibialis anterior (TA). **(B)** The model has three degrees of freedom distributed at the hip, knee and ankle joints. 6

3.1 Overview of single shooting optimization framework. The red dots in the open-loop controller represents the node points obtained from the discretization of the excitation trajectories of actuators. 11

3.2 $exp(t|\tau_{..})$ for ,$\tau = 0.2sec$ and $t_f = 1.6sec$ 12

3.3 Scalar α, used within the cost expressions, represents the percentage of STS completion and ranges between 0 to 1. The dashed circles show the states that are equidistant from the C_{goal}. 13

3.4 **(A)** Evolution of different costs and **(B)** their relative contributions to the total cost for the best candidates observed during optimization using the 0% strength deficit model. The costs were smoothed using a rolling average of 10 generations for this plot. 14

3.5 Joint angle **(A)** and muscle activation **(B)** trajectories obtained using the 0% strength deficit model with normal relative weights as listed in Table 3.1 and the relative weights increased individually by 10%. The resulting STS trajectories appear not very sensitive to relative weights. 15

4.1 The initial posture used to generate STS trajectories and the mean initial posture observed during experiments. The model was moved slightly forward for simulation to compensate for its non-actuated lumbar joint. 19

4.2 Joint angle trajectories from the experimental trials of the healthy adult. The beginning and the end of STS were defined as the points when hip flexion and hip extensions velocities smoothed with a rolling window of $0.1s$ grew respectively higher or lower than $20°/s$. 20

4.3 Muscle activation trajectories from the experimental trials of the healthy adult. 20

4.4 Seat and ground reaction force trajectories from the experimental trials of the healthy adult. 21

5.1 **(A)** Different postures observed during the 0% strength deficit model's STS transition and **(B)** the comparison of associated joint angle trajectories against experimental observations. The first vertical dotted line marks the point when the model lost contact with the chair, and the second vertical dotted line marks the posture with maximum hip flexion. 27
5.2 Muscle activation trajectories associated with the 0% strength deficit model's STS transition and those recorded experimentally. 28
5.3 **(A)** Evolution of COM position and **(B)** velocity for the 0% strength deficit model's STS transition. 28
5.4 The zero moment point (feet forces) and the body's COM trajectories from the 0% strength deficit model's STS transition. 29
5.5 **(A)** Feet and **(B)** seat contact forces observed during the STS trajectory of the 0% strength deficit model and the experiments. 29
5.6 **(A)** Postures , **(B)** external assistance and **(C)** muscle activation trajectories from the STS transition of the externally assisted 80% strength deficit model. The green arrow in **(A)** represents the resultant external assistance force. 30
5.7 Muscle activations, muscle forces, and their respective contributions to the resultant joint torques from the STS trajectories of 0%, 20%, 40% and 60% strength deficit models. 31

List of Tables

2.1 Muscles included in the models, their acronyms and their respective maximum isometric strengths for the base model. 8

3.1 Cost function hyperparameters 12

5.1 Properties of the 0%, 20%, 40%, 60% and externally assisted 80% strength deficit model's STS trajectories. Rows 5, 6, 8 and 9 show contributions of muscles to peak resultant joint torques. 32

List of Symbols

Symbol	Description
STS	Sit-to-stand
COM	Center of mass
VAS	Vastus muscle
GMAX	Gluteus maximus muscle
HAMS	Hamstrings muscle
ILPSO	Iliopsoas muscle
RF	Rectus Femoris muscle
GAS	Gastrocnemius muscle
SOL	Soleus muscle
TA	Tibialis Anterior muscle
t	time
$..(t)$	Value of a expression .. at time t
$\|..\|$	The absolute value expression ..
t_0	Simulation start time
t_f	Simulation final time
t_{max}	Upper limit of t_f
t_{SR}	Time of seat release
C_0	Center of mass position at t_0
C_f	Center of mass position at t_f
C_{goal}	Center of mass position for standing posture
$d(C_1, C_2)$	Euclidean distance between center of mass positions at t_1 ane t_2
α	% Sit to stand completion
$F_{chair,y}$	y component of constraint force applied by the chair on the femur head
τ	Time constant
a_i	Activation of actuator i
$e_{m,n}$	n^{th} excitation node of actuator m
$\|\|F_{Assist}\|\|$	Magnitude of external assistance
$T_{n,limit}$	Torque generated by the torsional limit spring at the n^{th} joint
$F_{feet,n}$	Component of force applied along n direction by the ground on the feet
ZMP_x	x coordinate of feet force zero moment point
$\dot{\theta}_j$	Velocity of joint j
$Feet_x$	x coordinate of the mid point between heel and toes
mg	Weight of musculoskeletal model

Chapter 1

Introduction

Sit-to-stand (STS) transition is a precursor to walking and, hence, critical for performing activities of daily life. It is also one of the most biomechanically challenging mobility tasks and, consequently, the first impediment to independent living for a large proportion of the elderly population. Lower extremity strength plays a vital role in human STS, and its deficits are thought to limit the STS functionality [Hughes et al., 1996, Schenkman et al., 1996, Gross et al., 1998, Meijer et al., 2009]. In this study, I identify the changes in STS caused by muscle strength deficits and investigate how they might lead to unsuccessful STS transition. I also present the external assistance trajectories that can complement strength deficits for successful STS transition.

The decline in muscle strength often co-occurs with other physiological and psychological impediments such as reduced balance, joint pain, and depression, making it difficult to access its independent effect on STS using experiments [Lord et al., 2002, Janssen et al., 2002]. Further, many extrinsic factors like foot placement, knee position, and chair height influence STS, making the standardization of experiments complex. Some past studies have used STS trajectories generated using optimization and human models to avoid the complications of experiments. Pandy et al. [1995] presented a cost function that generates STS trajectories with similar muscle activations to those of experiments. Bobbert et al. [2016] and Yokota et al. [2016] searched for trajectories that reduced loads on the muscles and the knee joint. However, the studies mentioned above have made either minimal or no observations about STS changes caused by strength deficits. Further, these studies have also not investigated how strength deficits might lead to unsuccessful STS.

Many older individuals incapable of independent STS transition can perform the same when assisted externally. This external assistance can help maintain or recover lower extremity strength when provided in an assist-as-needed manner. Thus it is desirable to generate reference assistance trajectories that assist as and when needed and by the amount that is needed. Mombaur and Hoang [2017] and Geravand et al. [2017] have used optimization to discover assistance trajectories that support part of the user's weight during STS and squat-to-stand motions, respectively. However, both the studies use human models with independently torque actuated joints. The hamstrings and the rectus femoris are two biarticular muscles that play an essential role in the STS transition [Millington et al., 1992, An et al., 2013, Hanawa et al., 2017]. Their biarticularity couples the torques produced at the hip and knee joints. This coupling should not be ignored, especially when generating reference

STS assistance trajectories, as it may lead to assistance profiles that over actuates one of these muscles, leading to muscle contracture and eventually lower back issues. The coupling is also crucial for accurately investigating the STS changes and the STS failure caused by the strength deficits. Thus, musculoskeletal models with varying degrees of strength deficits were used in this study to generate assisted and unassisted STS trajectories.

In this study, I have used single shooting optimization framework[1] to generate STS trajectories. Within the optimization framework, I have parameterized the open-loop excitation trajectories of the actuators similarly to Pandy et al. [1995], and Yokota et al. [2016]. The excitation trajectories are used to integrate the system's equation of motion of the equation forward in time to generate the resultant motion. The cost function evaluated on the resultant motion is then used to tune the actuator's excitation trajectories. Another possible optimization framework's structure is in whom the optimization is performed over the joint angle space. The tuning of joint angle trajectories is based on the solutions of inverse dynamics for skeletal models and the solutions of inverse dynamics and static optimization for musculoskeletal models. Such frameworks are used for STS synthesis in Sadeghi et al. [2013], Norman-Gerum and McPhee [2018], Yang and Ozsoy [2020], to discover STS trajectories with minimum actuator efforts in Yoshioka et al. [2007, 2012], and to predict the unilateral grab-rail assisted STS trajectories of a virtually unhealthy adult in Yang and Ozsoy [2021], Ozsoy and Yang [2021]. Direct collocation is another potential optimization framework. This framework performs optimization over both the joint angle and the actuator excitation space [Bobbert et al., 2016]. I selected open-loop single shooting trajectory optimization for its straightforward implementation and effortless extension to incorporate closed-loop controllers in future works.

It is difficult to identify and detail all of the parameters that shape the STS trajectories generated using optimization. For example, Bobbert et al. [2016], and Yokota et al. [2016] does not contain information about the initial guesses to the optimization algorithm, while Pandy et al. [1995] does not include information about the mechanical limits used to restrict the motion to the physiologically plausible range. Therefore I have made all the source code and results from this study public at https://github.com/ShibataLab/PredictiveSTS.

To enumerate the primary novelties of this work are:

1. an open-source single shooting optimization framework capable of generating assisted and unassisted STS trajectories.

2. use of optimization and musculoskeletal model to generate assisted STS trajectories.

3. predictions of the STS adaptations caused by strength deficits using optimization generated trajectories.

4. investigation of STS failure due to strength deficits.

The rest of the dissertation is organized into five chapters. In chapter 2, I detail the musculoskeletal models used in this study. Chapter 3 details the optimization

[1]For a brief introduction on trajectory optimization methods please use the following webpage: https://www.matthewpeterkelly.com/tutorials/trajectoryOptimization/canon.html

framework used to generate assisted and unassisted STS trajectories. In chapter 4 I detail the motion-tracking setup used to investigate the STS failure and the steps used to process the experimental data. Chapter 5 reports the findings of this study. Chapter 6 concludes this study with a summary of findings, identified limitations, and future research direction.

Chapter 2

Human Model

In this dissertation, the term human model is used for the mathematical representation of the human body's biomechanics. Human models can be classified as skeletal or musculoskeletal based on the actuation mechanics. Skeletal models have torque actuated joints, while musculoskeletal models have muscles that pull on different body segments. This study used musculoskeletal models for their more accurate actuation modelling compared to skeletal models.

Hamstrings and the rectus femoris are two biarticular muscles for whom significant activation have been experimentally observed in literature during STS transitions [Millington et al., 1992, An et al., 2013, Hanawa et al., 2017]. Their biarticularity couples the torques induced at the hip and knee joints. Hence it is critical to model it, especially for accurately investigating the STS failure or predicting external assistance trajectories that don't have undesirable muscle activations. I did not come across any study that modelled this coupling for a skeletal model during the literature survey. It motivated our selection for a musculoskeletal model instead of a skeletal one.

Musculoskeletal models with different strength deficits for this study were obtained by simultaneously scaling the maximum isometric strengths of the muscles present within the base model. For example, the 20% strength deficit model was obtained by multiplying the maximum isometric strengths of the base model by a factor of 0.8. The base model, also shown in Figure 2.1, is a simplified version of the LaiArnold2017 model [Lai et al., 2017]. The LaiArnold2017 model was selected since it is optimized for simulations that involve high hip and knee flexion. It represents an average-sized adult male of mass $75Kg$ and height $170cm$. The base model is 2D with 8 hill-type muscles and three degrees of freedom, while the source model is 3D with 80 hill type muscles and 37 degrees of freedom. The simplifications were needed to make the optimization problem computationally tractable. The following section detail some of these simplifications along with other modelling details.

2.1 Modelling simplifications

From the LaiArnold2017 model, the left leg and the associated muscles were removed. The masses of arms, forearms, hands and the head were lumped to the torso's center of mass (COM). The mass and inertia of the torso after lumping were halved to account for the missing left leg and the associated muscles. The right foot was fixed to the ground using a weld joint. Then the degrees of freedom cor-

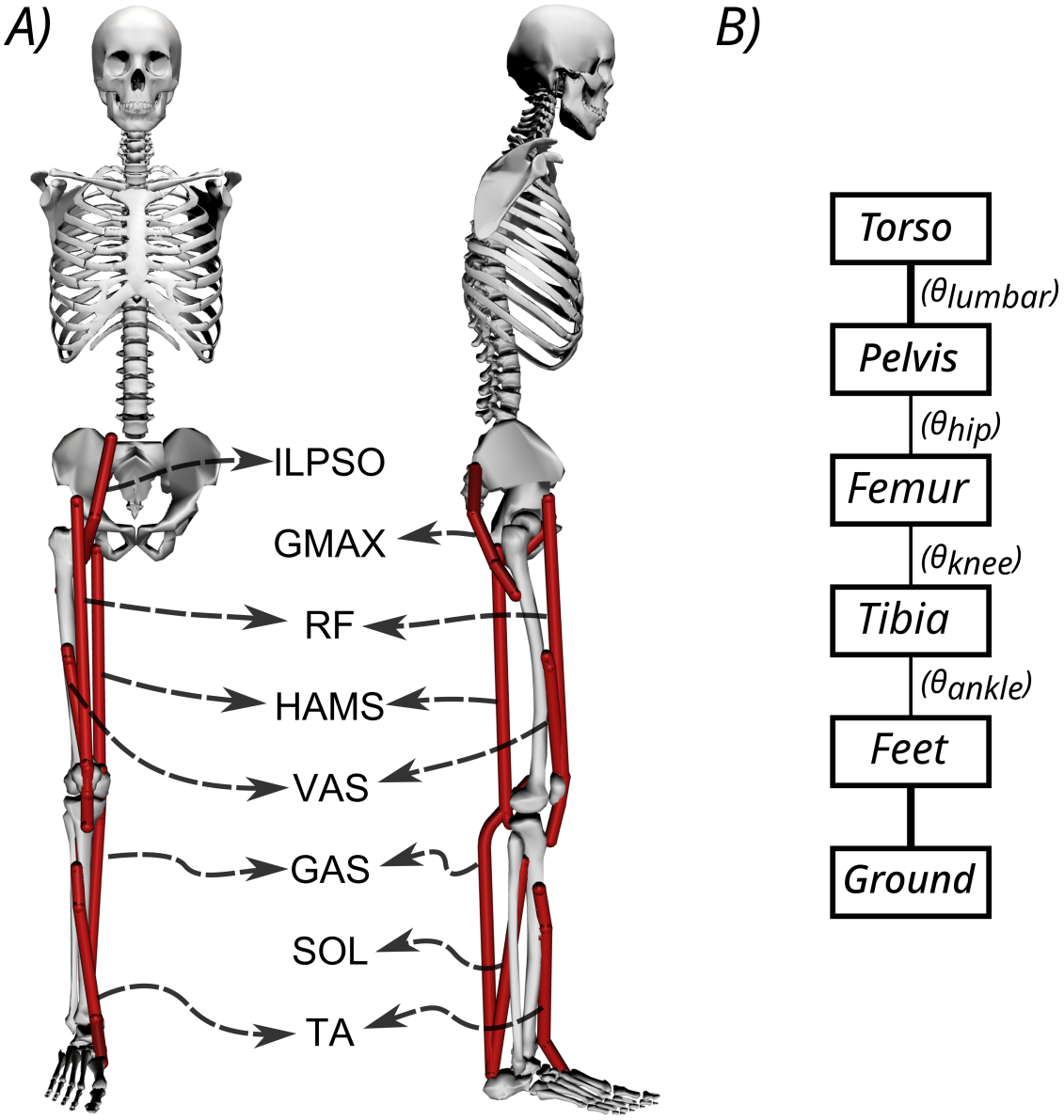

Figure 2.1: **(A)** A planar musculoskeletal model for sit-to-stand. The model's musculotendon actuators (red lines) represents the major uniarticular and biarticular muscle groups that drive the sit-to-stand motion in the sagittal plane, i.e., iliopsoas (ILPSO), gluteus maximus (GMAX), biarticular rectus femoris (RF), biarticular hamstrings (HAMS), vasti (VAS), gastrocnemius (GAS), soleus (SOL), and tibialis anterior (TA). **(B)** The model has three degrees of freedom distributed at the hip, knee and ankle joints.

responding to the sagittal plane motion of the ankle, knee, hip and lumbar joints were added. The 0° angle of the hip, knee, ankle and lumbar joints corresponds model standing upright. From 0°, the positive joint angles correspond to ankle dorsiflexion, knee flexion, hip flexion, and lumbar extension; and the negative joint angles correspond to the opposite. The lumbar joint was locked to $-10°$, for reasons explained in subsection 4.1 and thus, the model effectively has three degrees of freedom. The lower extremity muscles with similar functions were combined to single muscle-tendon units as realized in Ong et al. [2019]. Figure 2.1 shows insertion points and the paths of the resultant muscles included in the model, i.e., gluteus maximus (GMAX), biarticular hamstrings (HAMS), iliopsoas (ILPSO), biarticular rectus femoris (RF), vasti (VAS), biarticular gastrocnemius (GAS), soleus (SOL), and tibialis anterior (TA). Table 2.1 lists the maximum isometric strengths for the muscles included in the base model along with the acronyms. At the beginning of simulations, the muscle states were set by equilibrating the muscle-tendon units with the default activation of 0.05.

The chair-body contact interactions were modelled using a point on point kinematic constraint between the femur head and the chair. During simulation, the kinematic constraint was disabled if the vertical reaction forces required to maintain it turned non-compressive or satisfied the slipping condition. The seat kinematic constraint, once disabled, could not be re-engaged and thus prevented the optimization from getting stuck into local optima with multiple chair rises. The model had nonlinear torsional springs representing ligaments at the hip, knee, and ankle joints, limiting the motions to physiologically plausible ranges. They generated torques when the hip joint flex beyond 120°or extends below 30°, or the knee joint flex beyond 140° or extend beyond 0°, or the ankle dorsiflex beyond 30° or plantarflex beyond 40°. These ranges are from the LaiArnold2017 model. The remaining torsional spring parameters are from Ong et al. [2019].

External assistance was introduced at the torso's COM in the musculoskeletal model that failed to perform unassisted STS transition. The rationale behind introducing it at the torso is explained in subsection 5.3. For implementation simplicity, the external assistance was modelled using two independent point forces acting in the vertical and horizontal directions. Their respective magnitudes were limited to the 0-200 N range. Before computing actuation, the excitation signals to point forces were passed through first-order activation dynamics. It made the external assistance trajectories smooth and thus reduced the optimization framework's sensitivity to the values of individual assistance force decision variables. The first-order activation dynamics had a time constant of 0.1 *sec*. The OpenSim API [Delp et al., 2007] was used to formulate the musculoskeletal model's equation of motion and their forward integration.

Muscle	**Acronym**	**Maximum Isometric Strength (N)**
Iliopsoas	ILPSO	2697.3
Gluteus maximus	GMAX	3337.6
Biarticular Rectus Femoris	RF	2191.7
Biarticular Hamstrings	HAMS	4105.5
Vasti	VAS	9594.0
Biarticular Gastrocnemius	GAS	4690.6
Soleus	SOL	7925.0
Tibialis Anterior	TA	2116.8

Table 2.1: Muscles included in the models, their acronyms and their respective maximum isometric strengths for the base model.

Chapter 3

Optimization Framework

The optimization framework used the aCMA-ES algorithm [Arnold and Hansen, 2010]. aCMA-ES is a stochastic gradient-free optimization algorithm that adapts a Gaussian distribution towards low energy regions. It was selected for its enhanced robustness to locally optimal solutions than the gradient-based algorithms. The decision variables for the optimization framework were the simulation duration (t_f) and the node points ($e_{m,n}$) obtained by discretizing the actuator's excitation trajectories. I used the *libcmaes* library [CMA-ES, 2013] for the aCMA-ES algorithm.

An overview of the optimization framework used to generate STS trajectories in this study is shown in Figure 3.1. At each generation, aCMA-ES sampled a batch of candidate solutions (t_f, $e_{m,n}$) from the Gaussian distribution being adapted. Subsequently, open-loop actuator excitation trajectories were constructed for each candidate solution. Then, the musculoskeletal model's equation of motion were integrated forward in time using the open-loop actuator excitation trajectories as inputs to obtain the resulting motion. Then, the cost function values were evaluated for all the candidate solutions based on the respective resulting motions and passed on to the aCMA-ES algorithm. aCMA-ES then adapted the mean and covariance of Gaussian distribution based on the cost function values and samples the next batch of candidate solutions and so on until one of the stopping criteria is met. The following sections further details the different components of the optimization framework.

3.1 Optimization Setup

Piecewise linear functions with a fixed time step of 0.1 *sec* were used to discretize the excitation trajectories of the actuators present within the musculoskeletal model. The upper limit for simulation duration (t_{max}) was selected to be 1.6 *sec*, similar to Yokota et al. [2016]. All the musculoskeletal models had 8 hill-type muscles, and the externally assisted musculoskeletal model had two additional point actuators. At t_0, the actuators had their default activation. Thus, the optimization problem had 129 decision variables when generating unassisted STS trajectories and 161 decision variables when generating assisted STS trajectories.

As mentioned before, aCMA-ES is a stochastic gradient-free optimization algorithm that adapts a Gaussian distribution towards low energy regions. The node point values corresponding to the model sitting in a chair were used as the initial guess for the mean of the Gaussian. The algorithm was restarted if the number of

generations exceeded 4000 or if the improvement in the cost values was lower than 1.0 for the best candidate solutions over the immediate 250 generations. At each restart, the generation counter and the covariance matrix were reset to default, and the mean was set to the been-seen candidate solution till then. Four restarts were performed to account for the stochasticity of the optimization algorithm and the non-linearity optimization space before selecting the optimal candidate solution.

3.2 Cost Function

IThe cost function we selected to engender STS transition is a linear combination of ten different terms and can be expressed as follows:

$$\phi_{total} = \sum_{i=1}^{10} w_i \phi_i \tag{3.1}$$

where w_i is the relative weight of i^{th} cost term, i.e., ϕ_i. The mathematical expressions for the ten cost terms are given in Equations 3.2 - 3.12. Please refer to List of Symbols for the description of symbols used in these equations. All the elements associated with different costs were computed in SI units.

$$\phi_1 = \frac{d(C_f, C_{goal})}{d(C_0, C_{goal})} \tag{3.2}$$

$$\phi_2 = [1-\alpha] \int_{t_0}^{t_f} \frac{e^{t/\tau}}{\tau[e^{t_f/\tau} - 1]} F_{chair,y}(t) dt \tag{3.3}$$

$$\phi_3 = \sqrt{\frac{\sum\limits_i \int_{t_0}^{t_f} a_i(t)^2 dt}{\sum i}} \tag{3.4}$$

$$\phi_4 = \sqrt{\frac{\sum\limits_i \int_{t_0}^{t_f} \dot{a}_i(t)^2 dt}{\sum i}} \tag{3.5}$$

$$\phi_5 = \int_{t_0}^{t_f} ||F_{Assist}(t)|| dt \tag{3.6}$$

$$\phi_6 = \sum_n \int_{t_0}^{t_f} |T_{n,limit}(t)| dt \tag{3.7}$$

$$\phi_7 = \alpha \max_{\{t_0,t_f\}} (0, |F_{feet,x}(t)| - \mu F_{feet,y}(t)) \tag{3.8}$$

$$\phi_8 = \alpha \max_{\{t_0,t_f\}} |ZMP_x(t) - Feet_x(t)| dt \tag{3.9}$$

$$\phi_9 = \alpha \left[|\dot{\theta}_{hip}(t_f)| + |\dot{\theta}_{knee}(t_f)| + |\dot{\theta}_{ankle}(t_f)| \right] \tag{3.10}$$

$$\phi_{10} = \alpha \begin{bmatrix} |\max\limits_{\{t_{SR},t_f\}} (F_{feet,y}(t)) - mg| + \\ |\min\limits_{\{t_{SR},t_f\}} (F_{feet,y}(t)) - mg| + \\ |(F_{feet,y}(t_f)) - mg| \end{bmatrix} \tag{3.11}$$

$$\alpha = 1 - \frac{\min(d(C_f, C_{goal}), d(C_0, C_{goal}))}{d(C_0, C_{goal})} \tag{3.12}$$

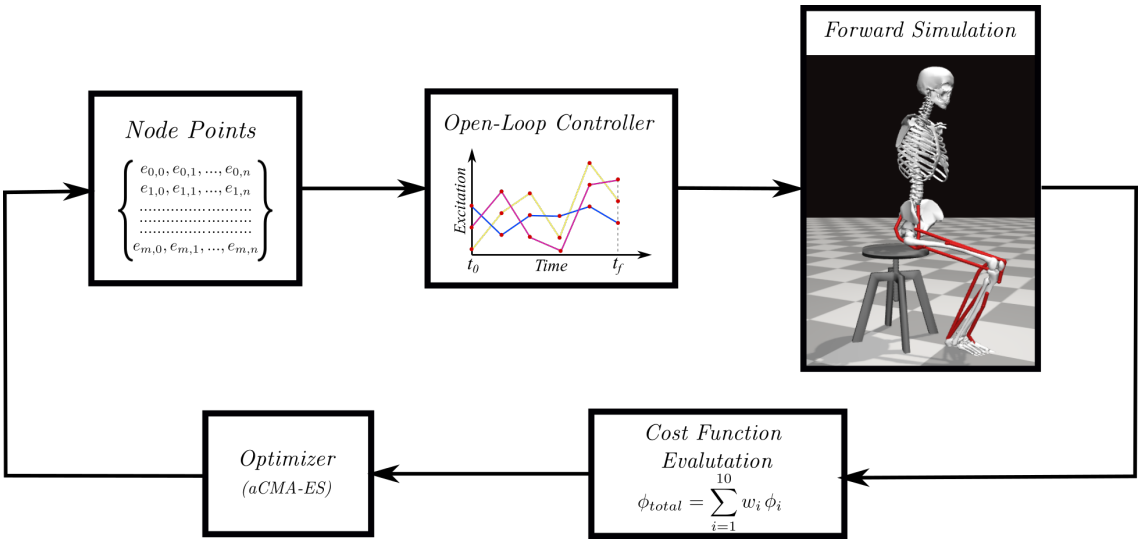

Figure 3.1: Overview of single shooting optimization framework. The red dots in the open-loop controller represents the node points obtained from the discretization of the excitation trajectories of actuators.

Cost ϕ_1 is the ratio of euclidean distances between the goal and t_f COM positions, and the goal and t_0 COM positions. The goal COM position corresponds to the model standing upright. Cost ϕ_2 penalizes the model staying in contact with the chair. Cost ϕ_2 features an increasing exponential (Figure 3.2) and thus penalizes the chair contact interactions more during the later part of simulation than prior. Costs ϕ_3 and ϕ_4 penalize the control effort and its rate of change, respectively. Cost ϕ_5 demotivates excessive use of external assistance. It was set to zero for the unassisted STS trajectories. Cost ϕ_6 discourages hyper-flexion and hyper-extension of joints. Costs ϕ_7 and ϕ_8 respectively penalize the feet contact forces that would lead to slip or tipping over the heel or toes. Cost ϕ_9 penalizes the body motion at t_f while cost ϕ_{10} penalizes the excessive body accelerations.

The scalar α represents STS progress and is illustrated in Figure 3.3. While learning to perform STS, the optimization first comes across unstable trajectories. Costs ϕ_7 to ϕ_{10} are scaled by α to prevent them from hindering the exploration of unstable STS trajectories for stable ones. It can be seen in Figure 3.4 that during the initial generations, the value of α is closer to zero as C_f is far away from C_{goal}. Then as the optimization progresses, cost ϕ_2 moves the model out chair and cost ϕ_1 moves it towards standing posture. This moves C_f towards C_{goal}, and the value of α and so the contribution costs ϕ_7 to ϕ_{10} increases. As the model learns to stand up, an increasing amount of control effort is required and thus, the relative contributions of costs ϕ_3 and ϕ_4 increase with optimization progress. The values of relative weights associated with different costs, i.e., w_i, were determined by trial and error and listed in Table 3.1 along with other cost function related hyperparameters. Figure 3.5 of the supplementary material shows the generated STS trajectories are not very sensitive to the w_i values.

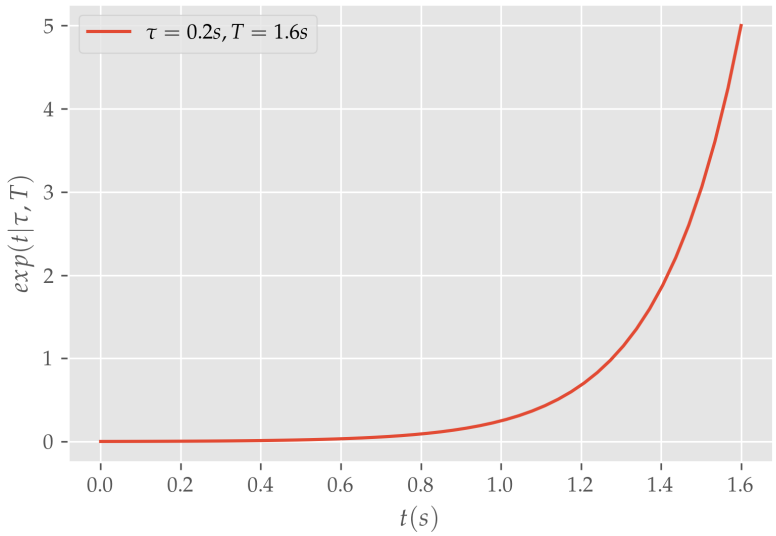

Figure 3.2: $exp(t|\tau_{..})$ for ,$\tau = 0.2sec$ and $t_f = 1.6sec$

Table 3.1: Cost function hyperparameters

Hyperparameters	**Value**
τ	$t_{max}/8$
w_1	800
w_2	1.2
w_3	175
w_4	70
w_5	5
w_6	10
w_7	0.1
w_8	1000
w_9	6
w_{10}	0.3

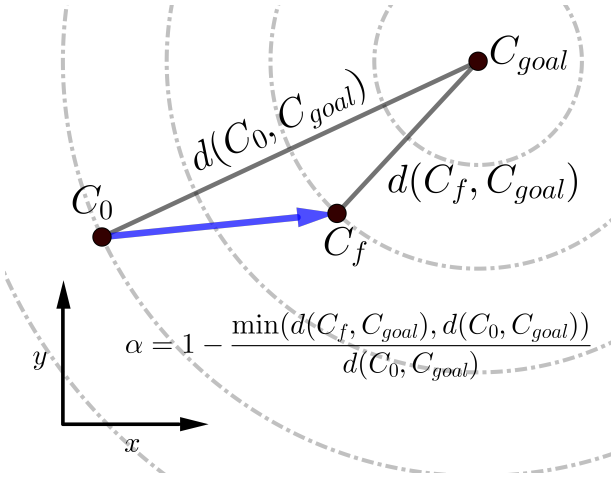

Figure 3.3: Scalar α, used within the cost expressions, represents the percentage of STS completion and ranges between 0 to 1. The dashed circles show the states that are equidistant from the C_{goal}.

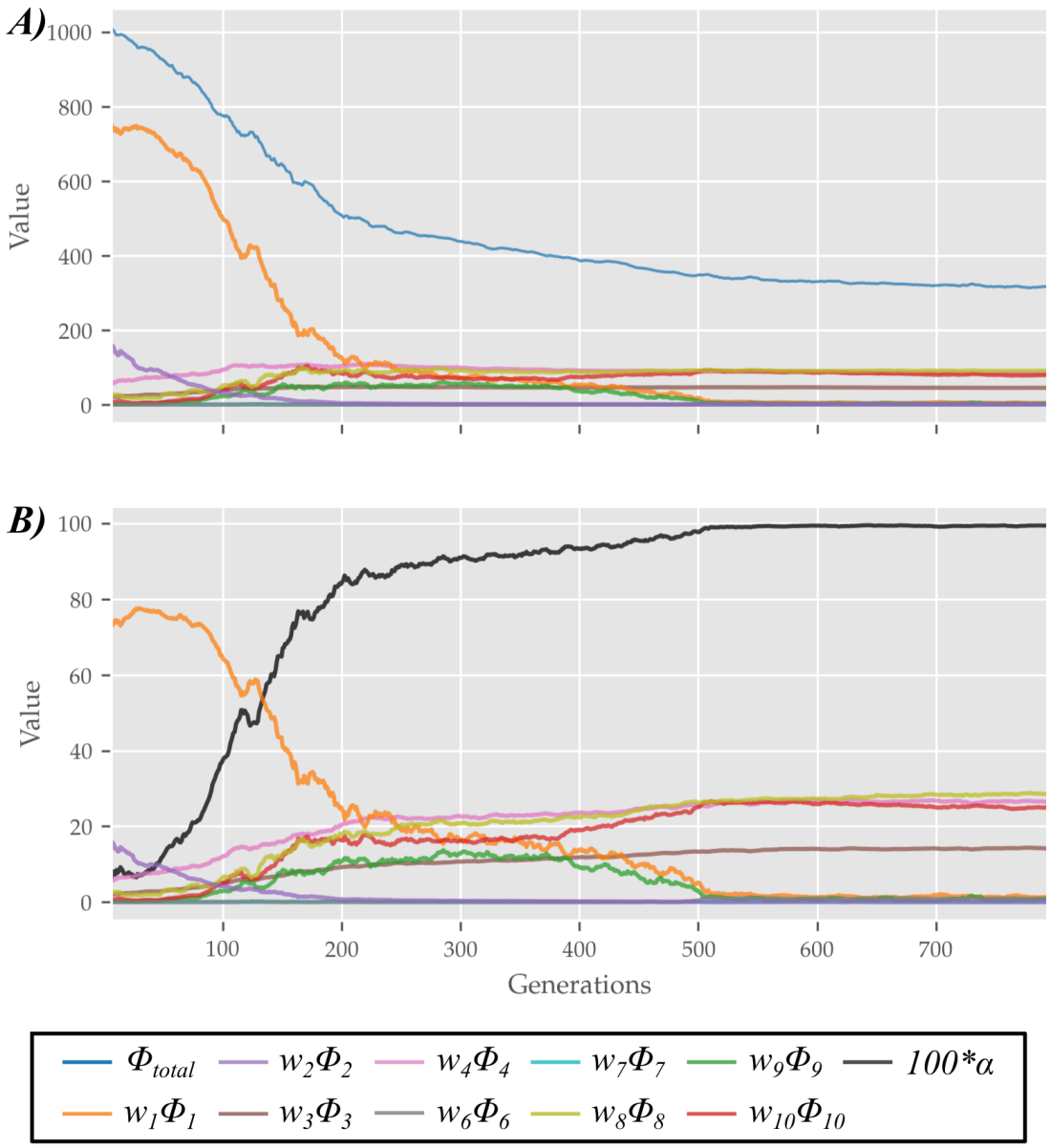

Figure 3.4: **(A)** Evolution of different costs and **(B)** their relative contributions to the total cost for the best candidates observed during optimization using the 0% strength deficit model. The costs were smoothed using a rolling average of 10 generations for this plot.

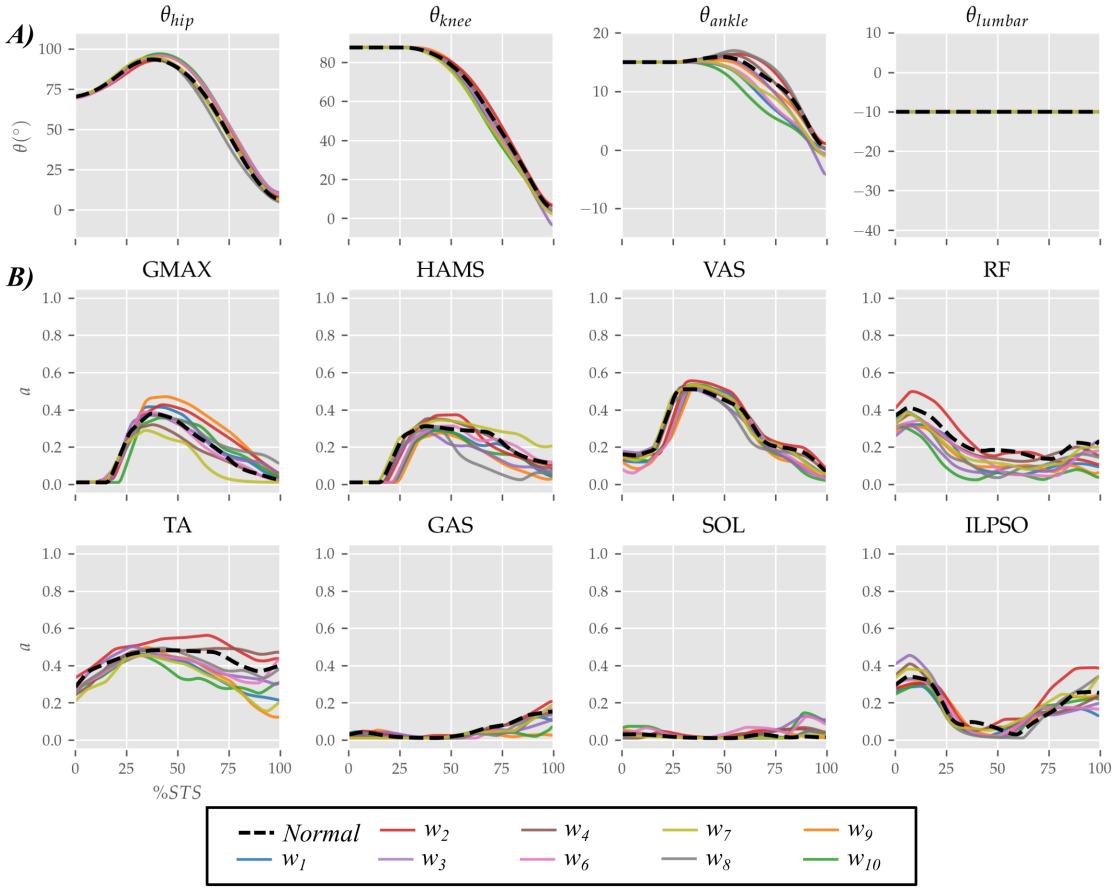

Figure 3.5: Joint angle **(A)** and muscle activation **(B)** trajectories obtained using the 0% strength deficit model with normal relative weights as listed in Table 3.1 and the relative weights increased individually by 10%. The resulting STS trajectories appear not very sensitive to relative weights.

Chapter 4

Analysis Tools

Experimental results observed for a healthy adult were used to validate the trajectories generated using optimization for the 0% strength deficit model. Section 4.1 details the steps used to process the experimental data. Motion tracking results were used to investigate the STS failure caused by strength deficits. Section 4.2 summarizes the motion tracking setup used for this purpose.

4.1 Experimental Data Processing

I have used the experimental data recordings of Lao et al. [2019] and Lao et al. [2020] to validate the 0% strength deficit model's STS trajectory generated. The experimental data contains optical marker trajectories, surface EMG signals and the ground and seat-pan reaction forces for 12 healthy adult subjects performing assisted and unassisted STS. Since the experimental data does not contain functional trials needed to scale musculoskeletal models, I have used the recordings of the subject with height and weight closest to our model. The selected subject weighs $71Kg$ and is $169cm$ tall. The source musculoskeletal model represents an adult male of mass $75Kg$ and height $170cm$.

The unassisted STS recordings have six trials under each of four conditions, i.e., arms folded across chest, arms hanging freely next to the body, natural STS, and slow pace imitating assisted STS. I used the 18 trials belonging to the first three categories. The optical markers were fixed to the musculoskeletal model on the average marker positions of the T-pose trial. This musculoskeletal model with registered optical markers was used for inverse kinematics. I defined the beginning and the end of STS as the times when hip flexion and hip extensions velocities smoothed with a rolling window of $0.1s$ were respectively higher or lower than $20°/s$. The resulting joint trajectories from the 18 trials are shown in Figure 4.2. The mean initial posture observed in experiments is compared to the initial posture used to generate STS trajectories in Figure 4.1. As can be observed, the simulation model was moved slightly forward towards the feet, and the lumbar joint was locked to $-10°$. The adjustments were made to compensate for the non-actuated lumbar joint. Also, the simulation's initial posture is easier to stand up from due to the torso lying closer to the feet.

The sEMG signals were processed by first passing through a fourth-order Butterworth bandpass filter with 10Hz and 350Hz cutoff frequencies. Then they were rectified and subsequently passed through a fourth-order Butterworth lowpass filter

of 3Hz cutoff frequency. Finally, the signals were normalized using the peak values from the maximum voluntary control trials. The ground and seat reaction force trajectories were not processed. Figures 4.3 and 4.4 respectively illustrate the sEMG and ground and seat reaction force trajectories from the 18 trails used in this study.

4.2 Motion Tracking Setup

The OpenSim Computed Muscle Control tool (CMC) was used to investigate the STS failure in this study. The CMC tool computes the actuator excitation levels at user-specified time intervals that will drive the generalized coordinates ($\vec{q}$) of the musculoskeletal model towards a desired kinematic trajectory ($\vec{q}_{\text{exp}}$) in the presence of external forces. At any given time t, the CMC tool first computes the desired acceleration $\ddot{\vec{q}}^*$ using the following proportional derivative control law:

$$\ddot{\vec{q}}^*(t+T) = \ddot{\vec{q}}_{\text{exp}}(t+T) + \vec{k}_v \left[\dot{\vec{q}}_{\text{exp}}(t) - \dot{\vec{q}}(t)\right] + \vec{k}_p \left[\vec{q}_{\text{exp}}(t) - \vec{q}(t)\right] \tag{4.1}$$

where, $\vec{k}_v$ and $\vec{k}_p$ are the feedback gains on the velocity and position errors, respectively. Since the forces that muscles apply cannot change instantaneously, the desired accelerations are computed some small-time T in the future. Then, CMC tool uses static optimization to distribute the load across synergistic actuators using static optimization. CMC tool offers two formulations for static optimization referred to as slow target and fast target. I used the fast target formulation. It minimizes the sum of squared controls augmented by a set of equality constraints which can be mathematically represented as follows:

$$J = \sum_{i=1} e_i^2 \tag{4.2}$$

$$C_j = \ddot{q}_j{}^* - \ddot{q}_j \qquad \forall j \tag{4.3}$$

where e_i is the control input/excitation of i^{th} actuator at time t and q_j is the j^{th} generalized coordinate. Since for many $\ddot{q}_j{}^*$ the muscles might not be able to produce sufficient forces, ideal torque actuators are added to the musculoskeletal model to prevent the fast target formulation from failing. Usually, the forces/torques produced per unit control effort for the ideal actuators is much lower than muscles. In such setups, following Equation 4.2, ideal torque actuators produce significant force/torque only when the muscles are saturated, and hence they are also referred to as reserve actuators.

To investigate the STS failure, I tracked the successful STS trajectory of the model with maximum strength deficit using the model for which the optimization framework failed to generate a successful STS trajectory. Since the CMC tool does not support event-based disabling of kinematic constraints, the seat forces were computed during the forward simulation and then supplied as external forces.

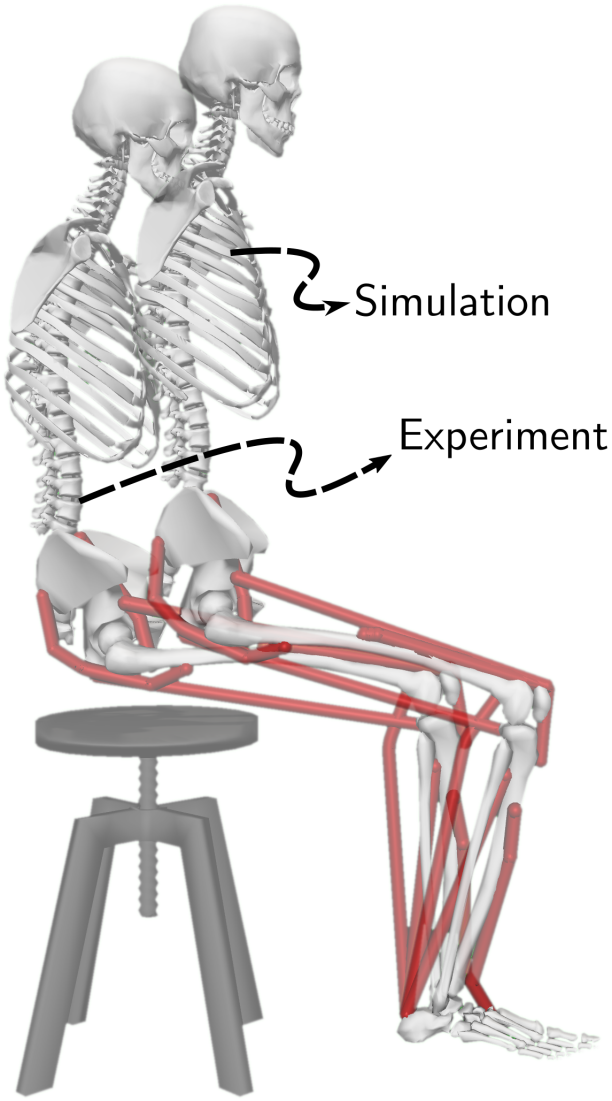

Figure 4.1: The initial posture used to generate STS trajectories and the mean initial posture observed during experiments. The model was moved slightly forward for simulation to compensate for its non-actuated lumbar joint.

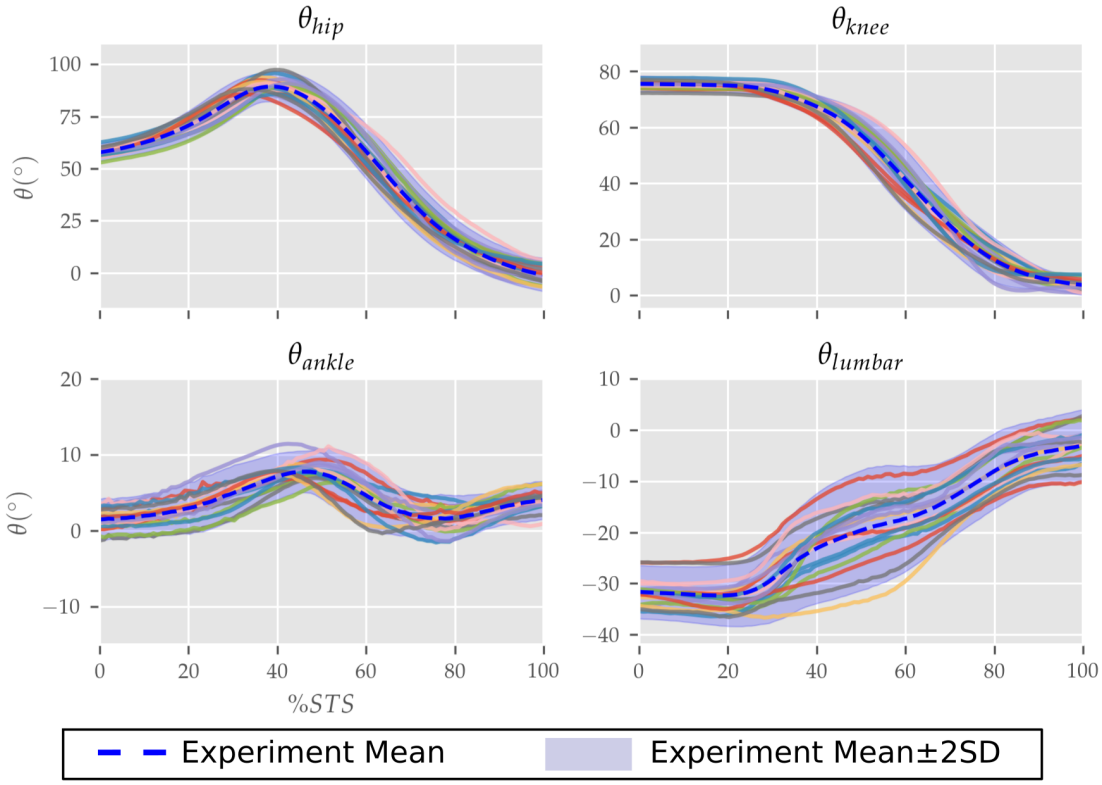

Figure 4.2: Joint angle trajectories from the experimental trials of the healthy adult. The beginning and the end of STS were defined as the points when hip flexion and hip extensions velocities smoothed with a rolling window of $0.1s$ grew respectively higher or lower than $20°/s$.

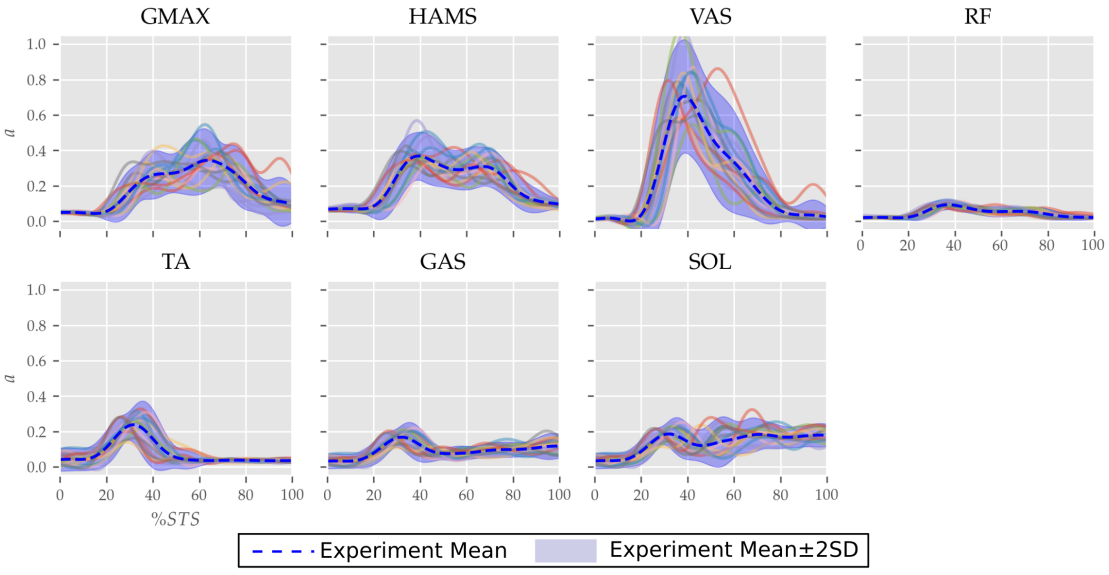

Figure 4.3: Muscle activation trajectories from the experimental trials of the healthy adult.

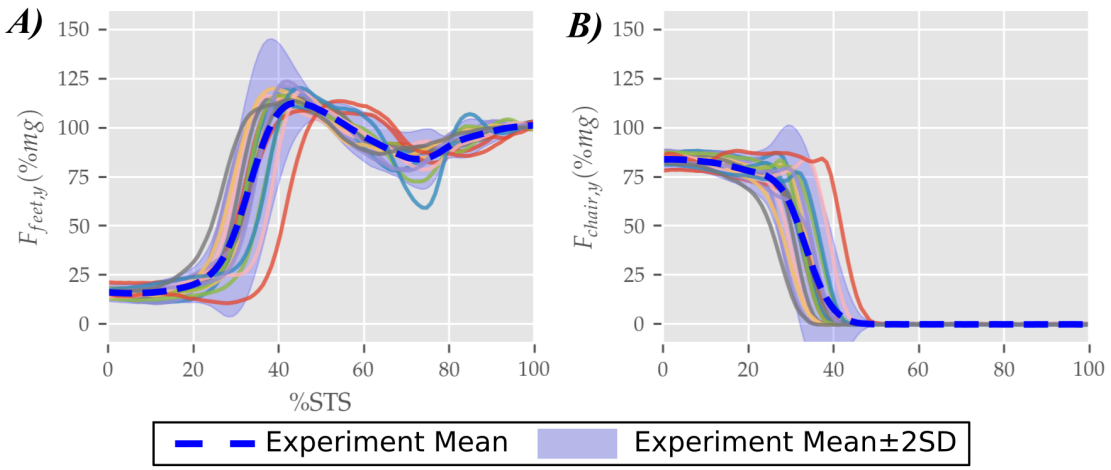

Figure 4.4: Seat and ground reaction force trajectories from the experimental trials of the healthy adult.

Chapter 5

Results

The optimization could generate successful STS trajectories for the 0%, 20%, 40% and 60% strength deficit models. However, for the 80% strength deficit model, the optimization could generate successful STS trajectories only when the model was assisted externally. The STS trajectories are divided into the three phases suggested in Millington et al. [1992] to facilitate discussions. Phase 1 starts with the trunk flexion and ends when the model loses contact with the chair. Phase 2 starts with the knee extension and ends when the hip joint is maximally flexed. Phase 3 begins with the reversal of trunk flexion to extension and ends with the model standing upright. The vertical black dotted lines in Figures 5.1-5.6 marks the transition between the three phases.

The results are organized into three sections. In subsection 5.1 the kinematics and dynamics of the 0% strength deficit model's STS trajectory are discussed and contrasted against the experimental observations. Subsection 5.2 details the adaptations and STS failure caused by muscle strength deficits. Subsection 5.3 discusses the features of the externally assisted 80% strength deficit model's STS trajectory. Please refer to Figures 5.1-5.7 and Table 5.1 during the following subsections for details. The resultant joint torques, in Figure 5.7 and Table 5.1, were obtained using inverse dynamical analysis of the STS trajectories. During inverse dynamical analysis, the muscles forces were excluded, while the seat constraint and assistance forces were supplied as external forces. The resultant joint torques and the contributions of different muscles to them were computed using OpenSim [Delp et al., 2007].

5.1 Unassisted STS Trajectory of 0% Strength Deficit Model

The joint angle, the muscle excitation, the COM position and velocity, the feet force zero moment point (ZMP), and the contact force trajectories associated with the 0% strength deficit model's STS trajectory are respectively illustrated in Figures 5.1 to 5.5. The STS motion is initiated by activating the ILPSO and RF muscles (Figure 5.2). Their activation generates torque around the hip joint and flexes the torso forward (Figure 5.7). It is followed by the deactivation of ILPSO and RF muscles and gradually increasing activations of the GMAX and HAMS muscles. Due to the trunk's forward flexion, the COM's horizontal velocity increases and peaks (Figure 5.3) before the activations of the GMAX and HAMS muscles increase to control the

torso's forward flexion. Also, the activation of VAS muscle increases to prepare for seat-off. Phase 1 ends when the VAS muscle has generated sufficient torques around the knee joint to lift the musculoskeletal model off the chair. The seat off takes place with the body's COM lying behind feet force ZMP (Figure 5.4). During phase 2, the GMAX and HAMS muscle activations increase until the hip flexion velocity reduces to zero. At this point, the trunk is maximally flexed, and phase 2 comes to an end. The knee joint extends only slightly during phase 2. The peak VAS, GMAX and HAMS muscle activations occur during phase 2. During phase 3, the activation of GMAX, HAMS, and VAS muscles slowly taper off because smaller forces are required to continue standing up due to an increasing fraction of body weight being borne by bone alignment. These patterns lead to the extension of both the hip and knee joints until the standing posture is achieved. At the end of phase 3, increased activation is observed in ILPSO, RF, and TA muscles to stop the hip, knee and ankle joints from extending past the upright posture. Also, during the latter half of phase 3, the body's COM reaches the feet support polygon. The SOL muscles see almost negligible activation; however, it produces significant passive fiber forces during the first two phases and a significant part of the third phase. Significant TA muscle activations are present during all three phases. These activations produce the force needed to balance the counteracting SOL and GAS muscle forces.

The joint angle trajectories of 0% strength deficits are contrasted against those observed experimentally for a healthy adult in Figure 5.1 **(B)**. The general shape of the hip and knee joint angle trajectories matches those of experiments. The discrepancies in the joint angle trajectories primarily result from the different initial postures (Figure 4.1). The mean initial posture from experiments requires the lumbar joint extension from -30° to nearly 0°. Our model did not include lumbar joint actuation for the reasons of modelling simplification. The initial posture was modified to compensate for the non-actuated lumbar joint by moving the model slightly forward and locking the lumbar joint with 10° of flexion.

The muscle activation patterns of the 0% strength deficit model's STS trajectory are compared to those of experiments in Figure 5.2. The general shape of activation patterns for the STS critical muscles, i.e., GMAX, HAMS and VAS, matches the experiments. The higher activation of VAS muscle than experiments during the first half of phase 1 is potentially due to cost term ϕ_2. Muscle RF features higher activation during STS initiation as the model did not feature trunk muscles. The higher activation of TA muscle than experiments is potentially due to the passive fiber forces induced in the SOL muscle by the initial posture. Experimental data features a small peak in the TA, GAS and SOL muscle activations during phase 2. This peak is absent in the generated STS. The experimental data did not include EMG signal for ILPSO muscle. The peak activations of all the muscles except RF and TA are within the two standard deviations of the peaks observed experimentally.

The seat and feet contact force trajectories of the 0% strength deficit model's STS transition are compared to the experimental observations in Figure 5.5. The lower seat-pan forces than experiments are most potentially because of the point on point constraint-based formulation. The flattening in the peak feet forces for simulation is because of the cost term ϕ_{10} and the absence of control noise. Also, the seat-off in simulation occurs earlier than in the experiments because the simulation's initial posture requires less horizontal momentum to stand up, and the kinematic constraint-based seat force formulation makes its development easier.

5.2 STS Adaptations and Failure

With strength deficits, the STS duration and the peak VAS, GMAX, RF, ILPSO and TA muscle activations increase (Table 5.1 and Figure 5.7). The peak HAMS muscle activation increases with muscle weakness up to 40% and then decreases for the 60%. The peak VAS muscle activation is higher than that of GMAX muscle up to 40% strength deficits and is equal for the 60% strength deficit. The decrease in the peak HAMS muscle activation from 40% to 60% strength deficit is to alleviate the saturated VAS muscle antagonistic at the knee joint. It is evident from the contribution of HAMS muscle to peak resultant knee torques dropping from -112.17% for the 40% strength deficit to -30.99% for the 60% strength deficit. The reduced HAMS muscle activation saturates the GMAX muscle as they work together to control the hip flexion. It is demonstrated by the contributions of HAMS muscle to the peak resultant hip torques dropping from 70.26% for the 40% strength deficit to 54.7% for the 60% strength deficit. Also, a reduction in the peaks of COM velocity, ground reaction forces, and GMAX, HAMS and VAS muscle forces is observed from the 40% to 60% strength deficits. Bobbert et al. [2016] also observes that with strength deficits, the STS duration increases, while the peak COM vertical velocity, peak GMAX, and VAS muscle forces decrease. However, Bobbert et al. [2016] does not observe any significant reduction in HAMS muscle activation. It is potentially because Bobbert et al. [2016] used the immediately prior solutions as the initial guess for the subsequent optimization. Besides STS duration and peak muscle activation, I did not observe consistent trends from the 0% to 40% strength deficits. It is most potentially because the optimizations converged to different locally optimal solutions for each model.

The optimization framework failed to generate STS transitions using the 80% strength deficit model. I suspected the GMAX or the VAS muscle to be responsible for this failure as they were getting saturated for the 60% strength deficit model's STS trajectory (Figure 5.7). I tracked the 60% strength deficit model's successful STS trajectory using the 80% strength deficit and two different reserve actuator setups. In the first setup, the optimal torque, i.e., torques generated per unit control effort, for the hip and knee torque actuators were $100Nm$ and $1Nm$ respectively, while for the second setup, they were $1Nm$ and $100Nm$. The first setup favored the utilization of the hip reserve actuator, while the second setup favored the utilization of the knee reserve actuator. The first setup's motion-tracking features a peak torque of $-19.81Nm$ by the knee reserve actuator and increased activation of both VAS and RF muscles. The second setup-based motion-tracking features a peak torque of $-12.05Nm$ by the hip reserve actuator and increased HAMS and GMAX activations. The lower magnitude of reserve actuator in the second setup suggests that the STS failure occurred because of VAS muscle weakness. Also, the observation that peak VAS muscle activation is greater than or equal to that of GMAX muscle supports this hypothesis.

5.3 Externally Assisted STS Transition

During the motion tracking of the previous subsection, it was observed that assisting the musculoskeletal model primarily at the hip joint lead to increased RF muscle activation, while assisting it primarily at the knee joint lead to increased HAMS

muscle activation. As STS transition is performed several times a day, assisting only at the hip or the knee joint has a high potential to cause the RF or the HAMS muscle contracture. Both the muscles cross the hip joint, and their contracture can cause back pain issues if not diagnosed. Thus the external assistance was introduced at the torso COM in the 80% strength deficit model. Also, assisting the model at the torso center of mass is a good approximation for assisting a human at the underarms area. The underarms area is easily graspable, and assistance using it helps simplify the design of probable STS assistance devices.

Physical assistance can help maintain or recover lower extremity strength when provided in an assist-as-needed manner. Thus while generating the assisted STS trajectories, the over-utilization of external assistance was penalized (Equation 3.6). Figure 5.6 shows the body postures, the assistance forces, and muscle activation for the externally assisted 80% strength deficit model's STS trajectory. The trajectory features utilization of external assistance when the VAS and GMAX muscle starts getting saturated, i.e., the model uses external assistance only when needed. The peak magnitudes of external assistance's vertical and horizontal components are 36.50% and 44.51% of the body's weight. The STS trajectory features reduced peaks of COM velocities, resultant hip and knee joint torques and the VAS, GMAX, and HAMS muscle forces. The seat-off takes place with the torso more upright than unassisted models.

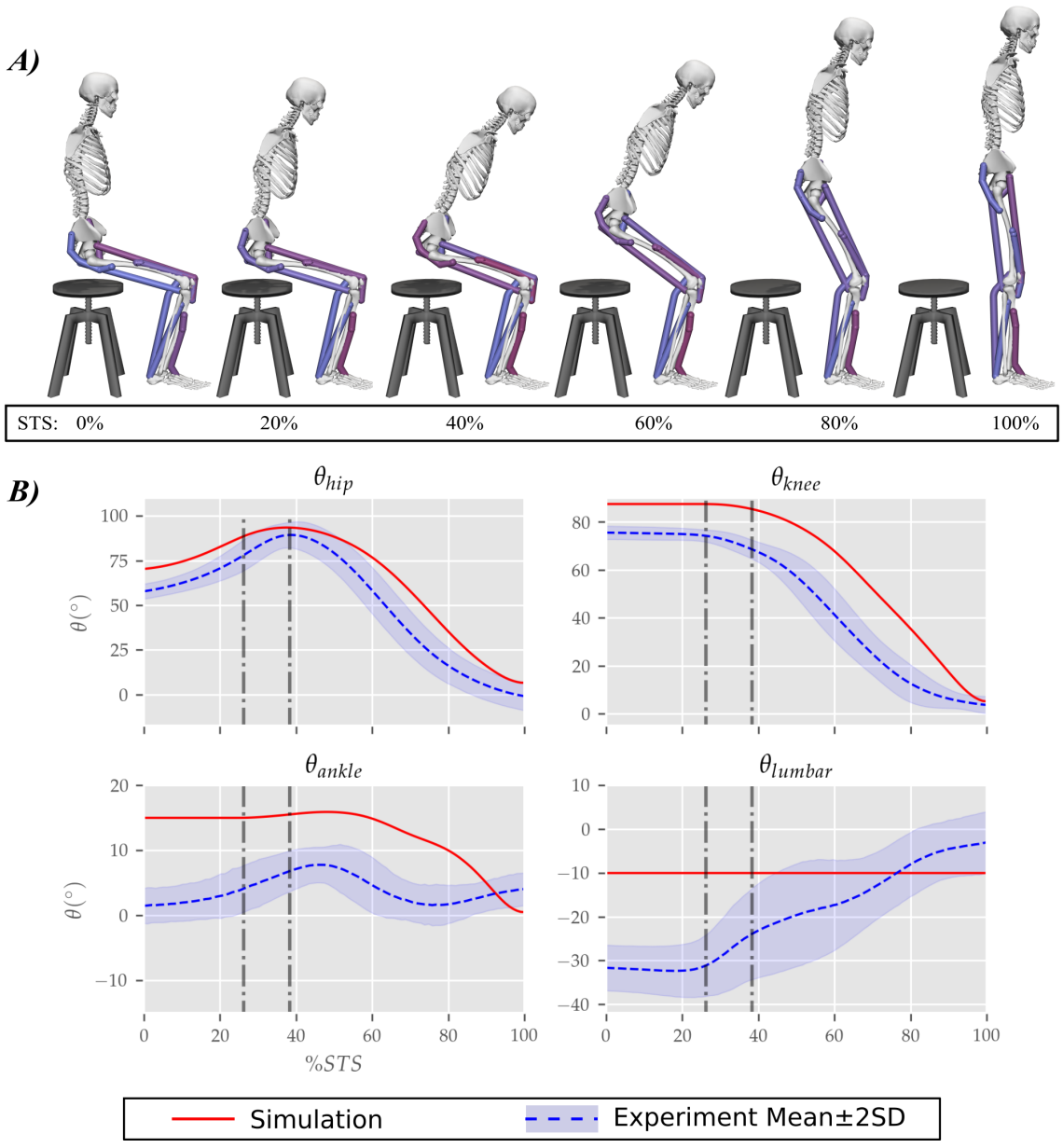

Figure 5.1: **(A)** Different postures observed during the 0% strength deficit model's STS transition and **(B)** the comparison of associated joint angle trajectories against experimental observations. The first vertical dotted line marks the point when the model lost contact with the chair, and the second vertical dotted line marks the posture with maximum hip flexion.

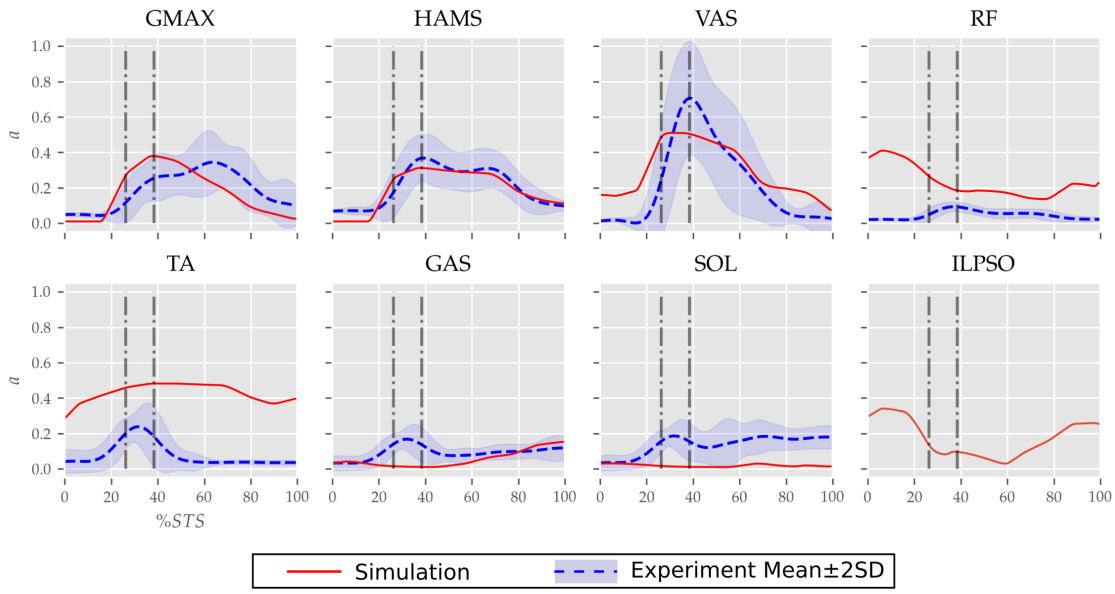

Figure 5.2: Muscle activation trajectories associated with the 0% strength deficit model's STS transition and those recorded experimentally.

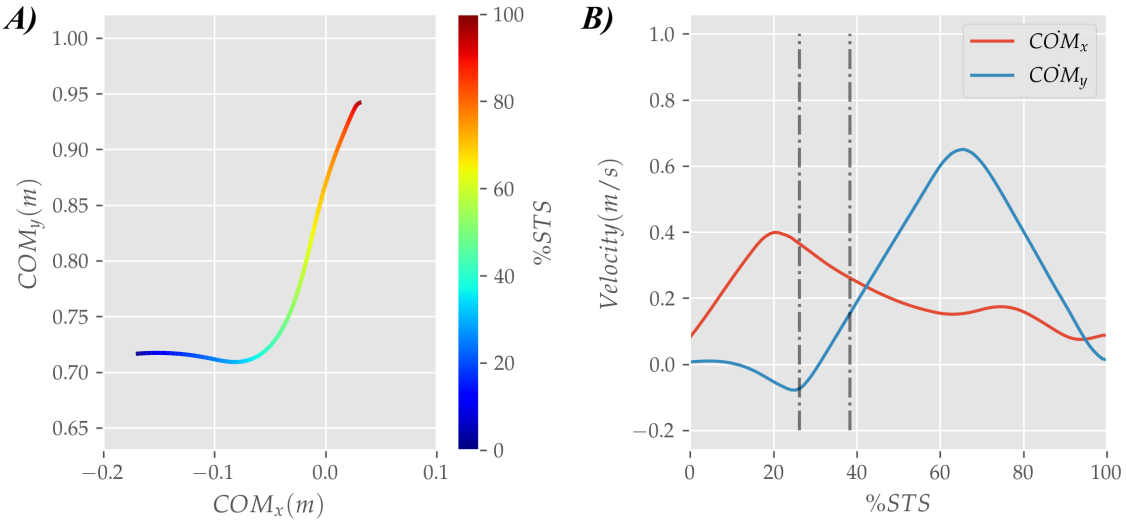

Figure 5.3: **(A)** Evolution of COM position and **(B)** velocity for the 0% strength deficit model's STS transition.

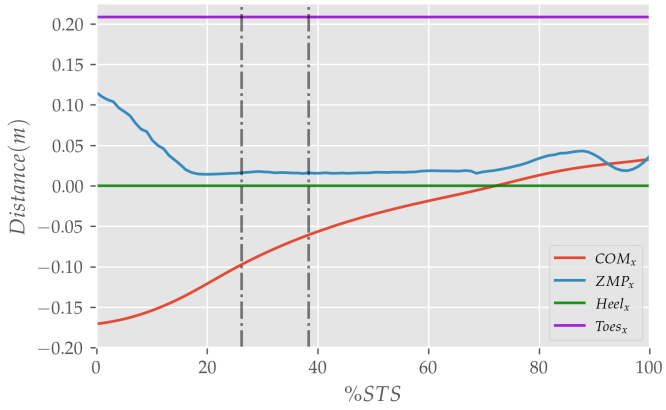

Figure 5.4: The zero moment point (feet forces) and the body's COM trajectories from the 0% strength deficit model's STS transition.

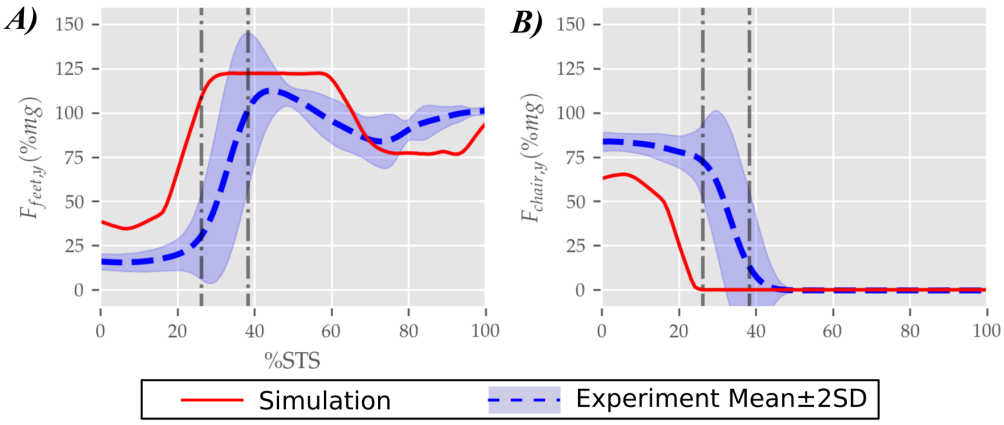

Figure 5.5: **(A)** Feet and **(B)** seat contact forces observed during the STS trajectory of the 0% strength deficit model and the experiments.

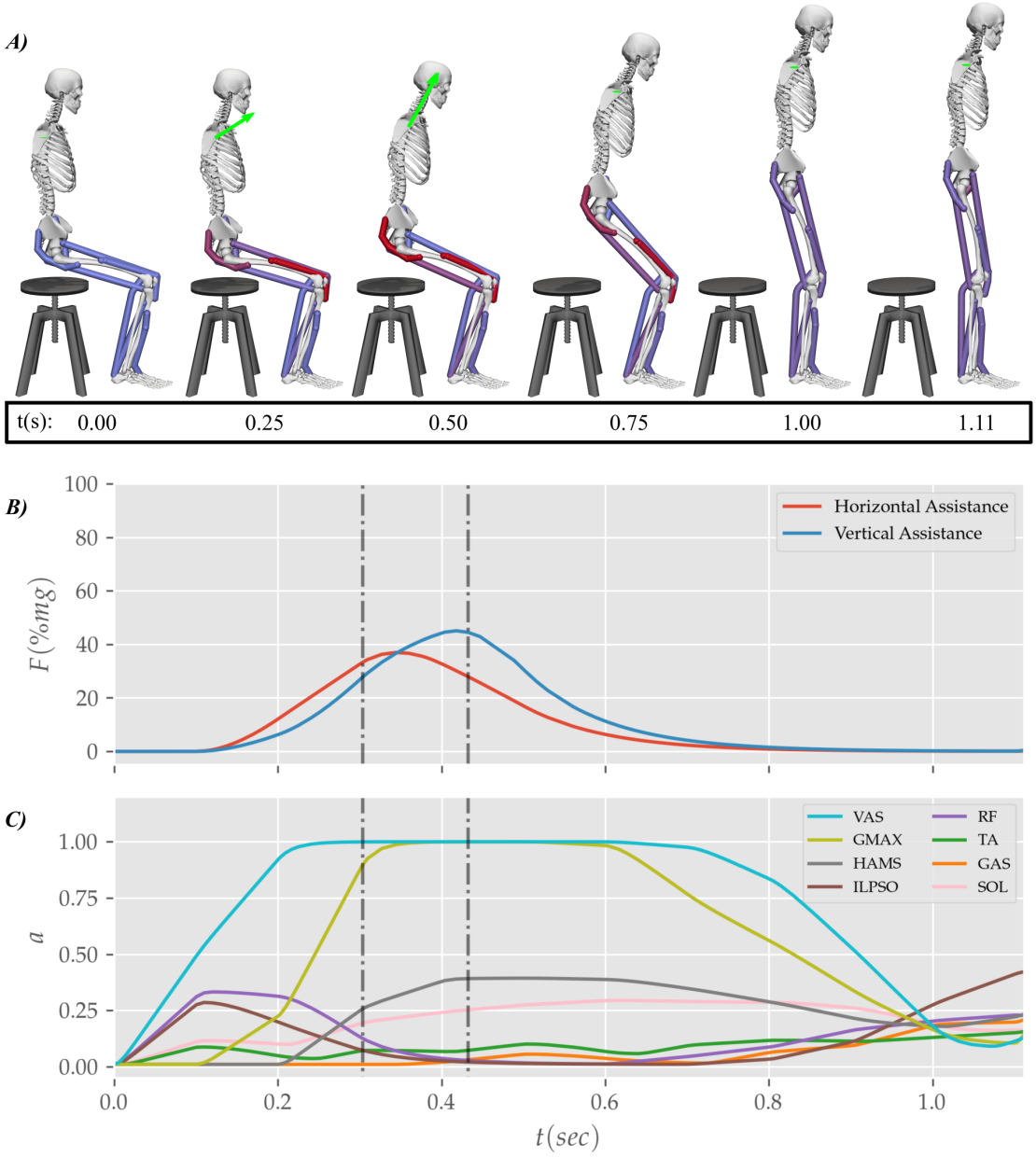

Figure 5.6: **(A)** Postures , **(B)** external assistance and **(C)** muscle activation trajectories from the STS transition of the externally assisted 80% strength deficit model. The green arrow in **(A)** represents the resultant external assistance force.

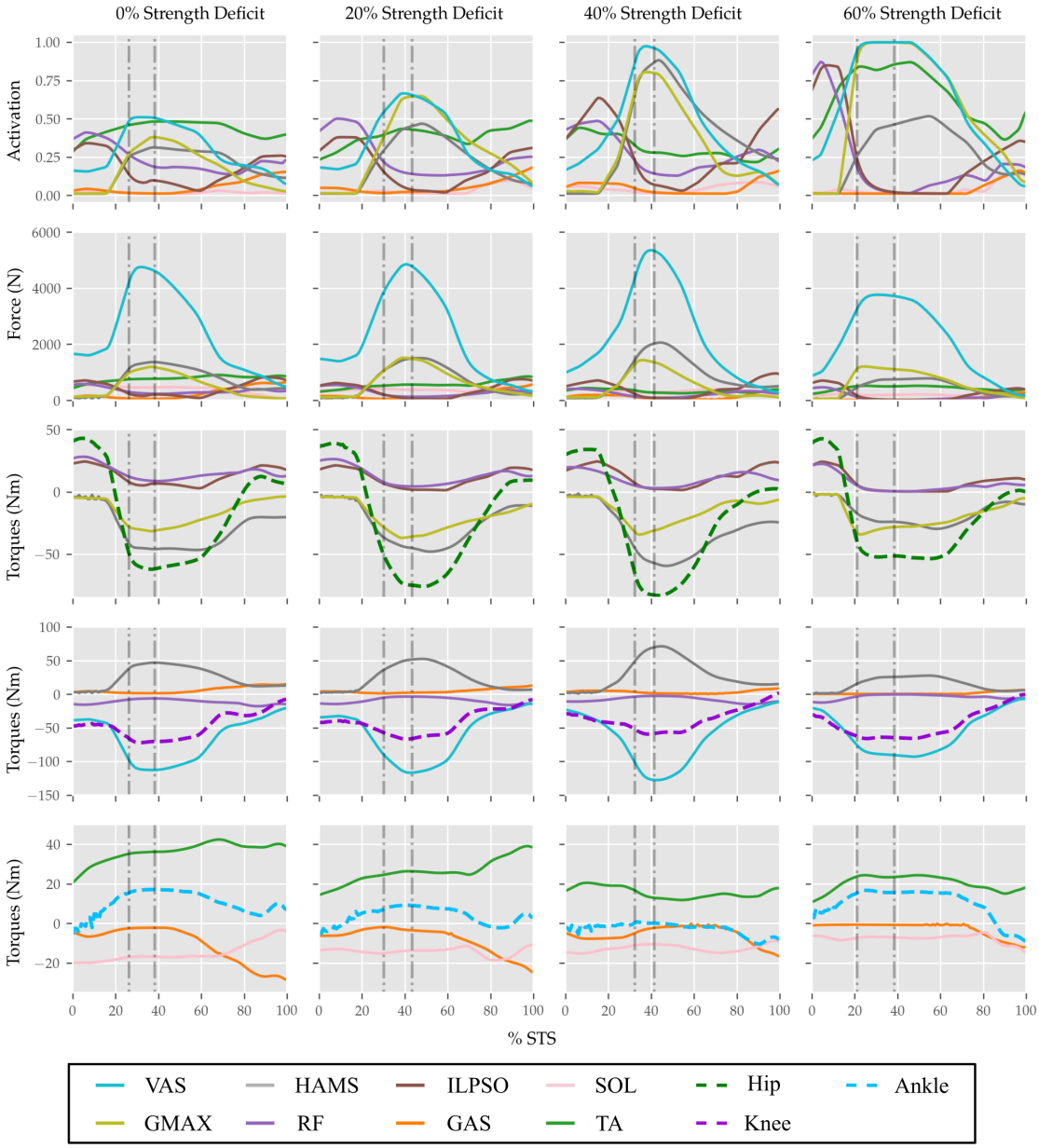

Figure 5.7: Muscle activations, muscle forces, and their respective contributions to the resultant joint torques from the STS trajectories of 0%, 20%, 40% and 60% strength deficit models.

Table 5.1: Properties of the 0%, 20%, 40%, 60% and externally assisted 80% strength deficit model's STS trajectories. Rows 5, 6, 8 and 9 show contributions of muscles to peak resultant joint torques.

#	**Property**	0% **Strength Deficit**	20% **Strength Deficit**	40% **Strength Deficit**	60% **Strength Deficit**	**80% Strength Deficit Assisted**
1	STS duration (s)	1.14	1.23	1.33	1.47	1.11
2	Peak COM Horizontal Velocity (m/s)	0.40	0.42	0.42	0.39	0.43
3	Peak COM Vertical Velocity (m/s)	0.65	0.71	0.65	0.55	0.42
4	Peak Hip Torque (Nm)	-62.17	-76.10	-83.28	-53.58	-35.59
5	GMAX Peak Hip Torque (Nm)	-31.60	-35.12	-30.03	-26.17	-20.96
6	HAMS Peak Hip Torque (Nm)	-45.91	-47.15	-58.51	-29.31	-15.44
7	Peak Knee Torque (Nm)	-72.02	-66.73	-59.22	-65.86	-42.19
8	VAS Peak Knee Torque (Nm)	-111.26	-115.92	-125.02	-85.51	-42.36
9	HAMS Peak Knee Torque (Nm)	44.40	50.34	66.43	20.41	2.69
10	Peak VAS Force (N)	4754.10	4857.40	5355.19	3765.91	1907.14
11	Peak GMAX Force (N)	1194.27	1513.42	1437.11	1206.33	615.33
12	Peak HAMS Force (N)	1366.03	1505.99	2058.45	782.31	340.31

Chapter 6

Conclusion

This paper presented and analyzed the sit-to-stand (STS) trajectories generated using an open-loop single shooting optimization and musculoskeletal models with different strength deficits. The strength deficits were introduced by simultaneously scaling the maximum isometric strength of all the muscles in steps of 20%. The optimization could successfully generate STS trajectories for models with up to 60%strength deficits. The muscle activation patterns for the 0% strength deficit model agree reasonably with the experimental observations for a healthy adult. A reduction in the peak HAMS muscle activation is observed when the VAS muscle, antagonistic across the knee joint, gets saturated due to the strength deficits. The reduced HAMS muscle activation saturated the GMAX muscle. After clinical validation, the reduced ratio of peak HAMS to GMAX muscle activation can be used to plan intervention. Then, the motion-tracking results were used to suggest the VAS muscle weakness to be responsible for optimization's failure to generate STS trajectories using the 80% strength deficit model. The motion tracking results were also used to motivate the introduction of external assistance at the torso's centre of mass (COM). The optimization could generate successful STS trajectories for the externally assisted 80% strength deficit model. The optimal trajectory featured the utilization of external assistance in an assist-as-needed manner. I have made the source code for optimization public to speed up the design of future assist-as-needed STS care devices. Finally, the findings of this study should be observed with caution as they have many inherent assumptions. The most significant among them are discussed in the following next paragraphs, followed by our probable future research directions.

Many experimental studies report that the elderly follow a stabilization strategy in which they move the body's COM over the feet support polygon before getting off the chair [Schenkman et al., 1990, Meijer et al., 2009, van Lummel et al., 2018]. Like the mean initial posture of our experiments, the stabilisation strategy requires significant lumbar motion. For our musculoskeletal model, the body's COM lies just $1.15cm$ inside the feet support polygon when the trunk is maximally flexed while maintaining chair contact. Thus the elimination of the lumbar joint and the feet-ground relative degree of freedom, even though also made by Pandy et al. [1995], Bobbert et al. [2016], and Yokota et al. [2016], might have been oversimplifications for predicting STS trajectories of the elderly adults.

The strength deficits were introduced by simultaneously scaling all the muscles' maximum isometric strength. However, the strengths of all the muscles do not

deteriorate by the same ratio. Also, scaling the maximum isometric forces is not the only way to introduce strength deficits. For example, the peak muscle activations could have been limited to the same effect. Thus the strength deficit modelling, even though made similarly by Bobbert et al. [2016] and Yokota et al. [2016], should be investigated for more accurate predictions.

I assumed a sagittal plane of symmetry. However, it has been shown that even for healthy adults, one leg is usually more dominant than the other [Caruthers et al., 2016]. Also, significant asymmetries may arise when one of the upper extremities grabs surfaces for assistance. Thus, the optimization framework needs to be extended to use the 3D musculoskeletal model to generate more realistic assisted and unassisted STS trajectories. Other musculoskeletal model-related critical assumptions that must be validated are simplifying the muscle groups to single musculotendon units and the control level decoupling of muscles.

Perfect coordination between the musculoskeletal model and the external assistance was assumed. It led to an optimal assisted STS transition with $1.11sec$ STS duration and is unrealistic to replicate. The optimization framework should be extended to include sensory noise and delay in external assistance formulation to synthesize realistically replicable STS trajectories. The maximum simulation duration needs to be extended beyond $1.6sec$. The chair height and the initial posture heavily influence the STS transitions, and the results of this study are a function of them.

The cost function used in this study is not unique in its capability to engender STS. Further, even for the selected cost function, the relative weights of the different cost terms should have been chosen using inverse optimal control. The relative weights were selected using trial and error because of the computationally demanding nature of the optimization. The generated STS trajectories are local optimal solutions of nonlinear non-convex optimizations. The optimization's failure to generate STS using the 80% strength deficit model might have been due to the unsuccessful search rather than muscle saturation.

I plan to design a kinematic events-based closed-loop STS controller in the future. I also plan to investigate the torque and muscle actuated lumbar joint models for STS trajectories with more accurate joint kinematics and dynamics. Finally, I intend to extend the optimization framework to include sensory noise and delay for the more realistic models of assist-as-needed STS care devices.

Bibliography

Michael A Hughes, Barry S Myers, and Margaret L Schenkman. The role of strength in rising from a chair in the functionally impaired elderly. *Journal of biomechanics*, 29(12):1509–1513, 1996.

Margaret Schenkman, Michael A Hughes, Greg Samsa, and Stephanie Studenski. The relative importance of strength and balance in chair rise by functionally impaired older individuals. *Journal of the American Geriatrics Society*, 44(12): 1441–1446, 1996.

MM Gross, PJ Stevenson, SL Charette, G Pyka, and R Marcus. Effect of muscle strength and movement speed on the biomechanics of rising from a chair in healthy elderly and young women. *Gait & posture*, 8(3):175–185, 1998.

Kenneth Meijer, Paul JB Willems, Hans HCM Savelberg, et al. Muscles limiting the sit-to-stand movement: an experimental simulation of muscle weakness. *Gait & posture*, 30(1):110–114, 2009.

Stephen R Lord, Susan M Murray, Kirsten Chapman, Bridget Munro, and Anne Tiedemann. Sit-to-stand performance depends on sensation, speed, balance, and psychological status in addition to strength in older people. *The Journals of Gerontology Series A: Biological Sciences and Medical Sciences*, 57(8):M539–M543, 2002.

Wim GM Janssen, Hans BJ Bussmann, and Henk J Stam. Determinants of the sit-to-stand movement: a review. *Physical therapy*, 82(9):866–879, 2002.

MG Pandy, BA Garner, and FC Anderson. Optimal control of non-ballistic muscular movements: a constraint-based performance criterion for rising from a chair. *Journal of Biomechanical Engineering*, 117:15, 1995.

Maarten F Bobbert, Dinant A Kistemaker, Marco Aurélio Vaz, and Marko Ackermann. Searching for strategies to reduce the mechanical demands of the sit-to-stand task with a muscle-actuated optimal control model. *Clinical Biomechanics*, 37:83–90, 2016.

Hiroki Yokota, Shigemichi Ohshima, and Naoki Mizuno. Sit-to-stand motion analysis using multiobjective genetic algorithm based on musculoskeletal model simulation. *IEEJ Journal of Industry Applications*, 5(3):236–244, 2016.

Katja Mombaur and Khai-Long Ho Hoang. How to best support sit to stand transfers of geriatric patients: Motion optimization under external forces for the design of physical assistive devices. *Journal of biomechanics*, 58:131–138, 2017.

Milad Geravand, Peter Zeno Korondi, Christian Werner, Klaus Hauer, and Angelika Peer. Human sit-to-stand transfer modeling towards intuitive and biologically-inspired robot assistance. *Autonomous Robots*, 41(3):575–592, 2017.

Pamela J Millington, Barbara M Myklebust, and Georgia M Shambes. Biomechanical analysis of the sit-to-stand motion in elderly persons. *Archives of Physical Medicine and Rehabilitation*, 73(7):609–617, 1992.

Qi An, Yuki Ishikawa, Junki Nakagawa, Hiroyuki Oka, Hiroshi Yamakawa, Atsushi Yamashita, and Hajime Asama. Analysis of contribution of muscle synergies on sit-to-stand motion using musculoskeletal model. In *2013 IEEE Workshop on Advanced Robotics and its Social Impacts*, pages 13–18. IEEE, 2013.

Hiroki Hanawa, Keisuke Kubota, Takanori Kokubun, Tatsuya Marumo, Fumihiko Hoshi, Akira Kobayashi, and Naohiko Kanemura. Muscle synergies underlying sit-to-stand tasks in elderly people and their relationship with kinetic characteristics. *Journal of Electromyography and Kinesiology*, 37:15–20, 2017.

Mohsen Sadeghi, Mehran Emadi Andani, Fariba Bahrami, and Mohamad Parnianpour. Trajectory of human movement during sit to stand: a new modeling approach based on movement decomposition and multi-phase cost function. *Experimental brain research*, 229(2):221–234, 2013.

Valerie Norman-Gerum and John McPhee. Constrained dynamic optimization of sit-to-stand motion driven by Bézier curves. *Journal of biomechanical engineering*, 140(12), 2018.

James Yang and Burak Ozsoy. Three dimensional unassisted sit-to-stand prediction for virtual healthy young and elderly individuals. *Multibody System Dynamics*, 49 (1):33–52, 2020.

Shinsuke Yoshioka, Akinori Nagano, Ryutaro Himeno, and Senshi Fukashiro. Computation of the kinematics and the minimum peak joint moments of sit-to-stand movements. *Biomedical engineering online*, 6(1):1–14, 2007.

Shinsuke Yoshioka, Akinori Nagano, Dean C Hay, and Senshi Fukashiro. The minimum required muscle force for a sit-to-stand task. *Journal of biomechanics*, 45 (4):699–705, 2012.

James Yang and Burak Ozsoy. Assisted Spatial Sit-to-Stand Prediction-Part 1: Virtual Healthy Elderly Individuals. *Journal of Computing and Information Science in Engineering*, 21(4):041002, 2021.

Burak Ozsoy and James Yang. Assisted Spatial Sit-to-Stand Prediction—Part 2: Virtual Injured Elderly Individuals. *Journal of Computing and Information Science in Engineering*, 21(6):061009, 2021.

Adrian KM Lai, Allison S Arnold, and James M Wakeling. Why are antagonist muscles co-activated in my simulation? A musculoskeletal model for analysing human locomotor tasks. *Annals of biomedical engineering*, 45(12):2762–2774, 2017.

Carmichael F Ong, Thomas Geijtenbeek, Jennifer L Hicks, and Scott L Delp. Predicting gait adaptations due to ankle plantarflexor muscle weakness and contracture using physics-based musculoskeletal simulations. *PLoS computational biology*, 15(10):e1006993, 2019.

Scott L Delp, Frank C Anderson, Allison S Arnold, Peter Loan, Ayman Habib, Chand T John, Eran Guendelman, and Darryl G Thelen. Opensim: open-source software to create and analyze dynamic simulations of movement. *IEEE transactions on biomedical engineering*, 54(11):1940–1950, 2007.

Dirk V Arnold and Nikolaus Hansen. Active covariance matrix adaptation for the (1+ 1)-CMA-ES. In *Proceedings of the 12th annual conference on Genetic and evolutionary computation*, pages 385–392, 2010.

CMA-ES. libcmaes. https://github.com/CMA-ES/libcmaes, 2013.

Bryan Lao, Tomoya Tamei, and Kazushi Ikeda. Characterizing Strategic Contributions of Physical Therapy to Natural Standing Motion in the Muscle Synergy Space. In *2019 41st Annual International Conference of the IEEE Engineering in Medicine and Biology Society (EMBC)*, pages 2311–2315. IEEE, 2019.

Bryan Lao, Tomoya Tamei, and Kazushi Ikeda. Data-Efficient Framework for Personalized Physiotherapy Feedback. *Frontiers in Computer Science*, 2:3, 2020.

Margaret Schenkman, Richard A Berger, Patrick O Riley, Robert W Mann, and W Andrew Hodge. Whole-body movements during rising to standing from sitting. *Physical therapy*, 70(10):638–648, 1990.

Rob van Lummel, Jordi Evers, Martijn Niessen, Peter Beek, and Jaap van Dieën. Older adults with weaker muscle strength stand up from a sitting position with more dynamic trunk use. *Sensors*, 18(4):1235, 2018.

Elena J Caruthers, Julie A Thompson, Ajit MW Chaudhari, Laura C Schmitt, Thomas M Best, Katherine R Saul, and Robert A Siston. Muscle forces and their contributions to vertical and horizontal acceleration of the center of mass during sit-to-stand transfer in young, healthy adults. *Journal of applied biomechanics*, 32(5):487–503, 2016.

Publication List

Kumar, V., Yoshiike, T., Shibata, T.
Predicting sit-to-stand adaptations due to muscle strength deficits and assistance trajectories to complement them
Frontiers in Bioengineering and Biotechnology, section Biomechanics, 2022.2.18